Chen *et al. Intell Robot* 2024;4:216-29
DOI: 10.20517/ir.2024.14

Intelligence & Robotics

Research Article

Open Access

Parameter identification of an open-frame underwater vehicle based on numerical simulation and quantum particle swarm optimization

Mingzhi Chen[1], Yuan Liu[1], Daqi Zhu[1], Anfeng Shen[2], Chao Wang[2], Kaimin Ji[2]

[1]School of Mechanical Engineering, University of Shanghai for Science and Technology, Shanghai 200093, China.
[2]Shanghai Maritime Surveying and Mapping Center, Shanghai 200090, China.

Correspondence to: Dr. Yuan Liu, School of Mechanical Engineering, University of Shanghai for Science and Technology, 516 Jungong Road, Yangpu District, Shanghai 200093, China. E-mail: 18903554308@163.com

How to cite this article: Chen M, Liu Y, Zhu D, Shen A, Wang C, Ji K. Parameter identification of an open-frame underwater vehicle based on numerical simulation and quantum particle swarm optimization. *Intell Robot* 2024;4:216-29. https://dx.doi.org/10. 20517/ir.2024.14

Received: 25 Apr 2024 **First Decision:** 23 May 2024 **Revised:** 19 Jun 2024 **Accepted:** 24 Jun 2024 **Published:** 26 Jun 2024

Academic Editors: Yueying Wang, Zengyuan Yin, Simon X. Yang **Copy Editor:** Pei-Yun Wang **Production Editor:** Pei-Yun Wang

Abstract

Accurate parameter identification of underwater vehicles is of great significance for their controller design and fault diagnosis. Some studies adopt numerical simulation methods to obtain the model parameters of underwater vehicles, but usually only conduct decoupled single-degree-of-freedom steady-state numerical simulations to identify resistance parameters. In this paper, the velocity response is solved by applying a force (or torque) to the underwater vehicle based on the overset grid and Dynamic Fluid-Body Interaction model of STAR-CCM+, solving for the velocity response of an underwater vehicle in all directions in response to propulsive force (or moment) inputs. Based on the data from numerical simulations, a parameter identification method using quantum particle swarm optimization is proposed to simultaneously identify inertia and resistance parameters. By comparing the forward velocity response curves obtained from pool experiments, the identified vehicle model's mean square error of forward velocity is less than 0.20%, which is superior to the steady-state simulation method and particle swarm optimization and genetic algorithm approaches.

Keywords: Underwater vehicle, parameter identification, numerical simulation, quantum particle swarm optimization, dynamic fluid-body interaction

1. INTRODUCTION

After prolonged operation, marine structures such as ships and offshore platforms may develop rust and corrosion on their surfaces due to biofouling and seawater corrosion[1]. Underwater vehicles have broad prospects for applications in the inspection, detection, cleaning, and maintenance of underwater structures such as ship hulls[2]. These tasks often require underwater vehicles to have stable, high-precision intelligent controllers to ensure stable imaging and detection operations. However, to design intelligent controllers and improve the control accuracy of underwater vehicles, it is often necessary to conduct parameter identification of underwater vehicle models to provide accurate reference models for the controllers[3]. Underwater vehicle model identification methods can be divided into two categories: non-parametric and parametric identification, including empirical formula method, constrained model test method, measured data identification method, numerical simulation method [e.g., computational fluid dynamics (CFD)], and so on. When using the empirical formula method to calculate the parameters of underwater vehicles, the empirical formulas of submarines and torpedoes are often borrowed for approximation calculation. Nevertheless, this is not applicable to open-frame underwater vehicles. The constrained model test method is a relatively precise approach for identifying underwater vehicle parameters. However, it suffers from drawbacks such as long model production cycles and high costs[4].

The experimental data identification method is to use the underwater vehicle data recorded in the experiment. Firstly, the data is pre-processed, and then the system identification of the underwater vehicle is completed by the least squares algorithm, neural network algorithm, genetic algorithm (GA), particle swarm optimization (PSO) algorithm, and so on[4-6]. Wang *et al.* utilized experimental data to construct an underwater vehicle model using long short-term memory (LSTM) and Q-learning[7], which is a non-parametric identification method. Due to the existence of parametric uncertainty in underwater vehicles, van de Ven *et al.* added a neural network to predict the unknown parameters on the basis of known hydrodynamic parameters, which simplified the training of the neural network and allowed for online and parallel learning of the unknown parameters[8], but the neural network online identification model has the disadvantage of large computational volume. In addition, many underwater vehicles do not carry velocity sensors, such as Doppler velocimeters, to provide the complete data needed for parameter identification, and there are also problems such as varying accuracy of sensors and accuracy of data sources.

Chocron *et al.* conducted underwater vehicle hydrodynamic parameter identification based on genetic algorithm and verified the excellent robustness and global optimality-seeking characteristics of GA[9]. Cardenas *et al.* used empirical formulas to obtain the initial hydrodynamic parameters and then proposed an online parameter correction method based on dilated Kalman filtering through the recorded underwater vehicle motion data[10]. Lin *et al.* conducted pool experiments using Ultra-wideband (UWB) positioning and HWT905 electronic compass, measured the linear and angular velocity response data of the underwater vehicle in the horizontal plane, and proposed a parameter identification method integrating the least-squares method and particle swarm optimization algorithm[11]. This method could only obtain the dynamics parameters of the underwater vehicle in the horizontal plane, but high accuracy is obtained. Prawin *et al.* proposed a quantum PSO method for nonlinear system parameter identification[12,13], but its potential application to underwater vehicles remains an open research direction.

The use of numerical simulation methods to handle viscous flow problems for underwater vehicle parameter identification offers advantages such as low cost and ease of implementation. The accuracy of numerical simulation methods is greatly related to the computational effort. With the improvement of computer performance and the development of industrial software, the speed and accuracy of the dynamic mesh technology and dynamic process numerical solutions have been effectively enhanced. Consequently,

an increasing number of researchers are employing numerical simulation methods to conduct hydrodynamic parameter identification for underwater vehicles. Based on STAR-CCM+, Zhou *et al.* proposed a numerical simulation method to address the identification of drag coefficients, including rotation, and obtained a high-precision model for controller design[14]. Hong *et al.* validated the hydrodynamic characteristics of a micro underwater vehicle by CFD[15]. Bentes *et al.* used CFD methods to carry out parameter identification of an underwater vehicle, but the acceleration parameters were obtained using an empirical method based on analytic methods[16]. Similarly, Wang *et al.* used slice theory to solve for the added mass and employed the CFD method to obtain resistance models for accessories such as the horizontal and vertical rudders of underwater vehicles, thereby achieving a more accurate model of the underwater vehicle[17]. However, the empirical formulation of slice theory is not applicable to open-frame underwater vehicles. Bao *et al.* identified the hydrodynamic parameters of the underwater vehicle based on the CFD and the least square method[18]. Di conducted resistance parameter identification for underwater vehicles using the steady-state calculation method based on STAR-CCM+[19].

Most of the CFD methods used in the above studies are limited to the parameter identification of viscous drag and most of them only perform single-degree-of-freedom steady-state numerical simulations after decoupling. STAR-CCM+ integrates geometry processing, meshing, physical solving, post-processing, *etc.*, which allows for convenient fluid computations and is widely used among researchers. Therefore, this paper proposes a study on the identification of full parameters of inertia and resistance for underwater vehicles using the overlapping grid and dynamic fluid-body interaction (DFBI) model based on the STAR-CCM+. On the four controllable degrees of freedom of the studied underwater vehicle, external forces are applied to the underwater vehicle to conduct transient simulations and obtain the velocity response curves for each degree of freedom. Based on the computed data, a parameter identification method using quantum particle swarm optimization (QPSO) is proposed. Experimental validation confirms that the proposed method is highly accurate and meets the requirements for controller design. The innovation and contribution can be summarized as follows. Unlike previous studies that mainly used CFD methods to obtain viscous hydrodynamic parameters, this article proposes using the DFBI model to calculate the velocity response of underwater vehicles under different forces and torques, and using QPSO to obtain the full hydrodynamic parameters (inertia and viscous parameters) of underwater vehicles, making it more convenient to use CFD to model underwater vehicles. The proposed method has higher accuracy compared to least squares, PSO, and GA algorithms, with a mean square error of 0.2%, which is smaller than other methods.

2. DYNAMIC MODELLING OF UNDERWATER VEHICLES

The dynamic modeling of an underwater vehicle is the foundation for the parameter identification. The underwater vehicle moves under the action of the thrust from the propellers, the resistance of the fluid, the added mass force, *etc.* According to Newton's laws, the six-degree-of-freedom dynamic model of the underwater vehicle can be established as[20].

$$(M_{RB} + M_A)\dot{v} + (C_{RB}(v) + C_A(v))v + D(v)v + g(\eta) = \tau \tag{1}$$

Where $v = [v_1\ v_2]$ is the velocity of the underwater vehicle; $\tau = [X\ Y\ Z\ K\ M\ N]$ represents the combined force and torque from the propellers; M_{RB} indicates the rigid body mass and inertia matrix; M_A denotes the added mass and inertia matrix; $C_{RB}(v)$ points to the rigid Coriolis and centripetal force matrix, $C_A(v)$ stands for the Coriolis and centripetal force matrix generated by the added mass; $D(v)$ corresponds to the fluid resistance coefficient matrix, $g(\eta)$ means the combined force of gravity and buoyancy.

Generally, after weight balancing, an underwater vehicle has only a small positive buoyancy, and its gravity and buoyancy forces essentially cancel each other out, set $g(\eta) = 0$. The designed underwater vehicle is controllable only in four degrees of freedom: x, y, z-direction translation and z-direction rotation. x- and y-direction rotations (transverse and longitudinal rolls and tilts) are kept in equilibrium by weight balancing and are not controlled by driving force; therefore, in this paper, we simplify the 6-degree-of-freedom model into 4-degree-of-freedom dynamics model as in Equations (2)-(7).

$$(M_{RB} + M_A)\dot{v} + (C_{RB}(v) + C_A(v))v + D(v)v = \tau \tag{2}$$

Assuming that the center of gravity of the underwater vehicle is at the origin, with coordinates (0, 0, 0), then:

$$M_{RB} = \mathrm{diag}\{m \quad m \quad m \quad I_{zz}\} \tag{3}$$

$$M_A = -\mathrm{diag}\{X_{\dot{u}} \quad Y_{\dot{v}} \quad Z_{\dot{w}} \quad N_{\dot{r}}\} \tag{4}$$

$$D(v) = -\mathrm{diag}\{X_u + X_{u|u|}\left|u\right|, Y_v + Y_{v|v|}\left|v\right|, Z_w + Z_{w|w|}\left|w\right|, N_r + N_{r|r|}\left|r\right|\} \tag{5}$$

$$C_{RB}(v) = \begin{bmatrix} 0 & 0 & 0 & -mv \\ 0 & 0 & 0 & mu \\ 0 & 0 & 0 & 0 \\ mv & -mu & 0 & 0 \end{bmatrix} \tag{6}$$

$$C_A(v) = \begin{bmatrix} 0 & 0 & 0 & Y_{\dot{v}}v \\ 0 & 0 & 0 & -X_{\dot{u}}u \\ 0 & 0 & 0 & 0 \\ -Y_{\dot{v}}v & X_{\dot{u}}u & 0 & 0 \end{bmatrix} \tag{7}$$

$C_{RB}(v)$ and $C_A(v)$ can be subsequently determined after the rigid mass and additional mass are determined. Therefore, the parameter identification for the underwater vehicle in this paper involves determining the rigid body mass matrix, added mass matrix, and drag coefficient matrix so that the thrust-velocity response of the established numerical model of the underwater vehicle matches the actual measured thrust-velocity response as closely as possible. The solution to Equation (2) can be set as Equation (8), and the objective function for model parameter identification is Equation (9), to minimize the 2-paradigm number of the difference between the measured speed and the model output speed.

$$v = f\left(\tau, M_{RB}, M_A, D\left(v\right)\right) \tag{8}$$

$$\underset{M_{RB}, M_A, D(v)}{\mathrm{argmin}} \quad \|\hat{v} - v\|_2 \tag{9}$$

Where $\hat{v}$ is measured velocity, and $\mathcal{V}$ is the calculated output of the model. In the calculation process, the thruster is considered as a non-rotating floating body, so the same approach to approximate simplification of the model as in the literature[21] is adopted for the additional mass parameters of the vehicle.

3. IDENTIFICATION OF MODE

This paper employs a CFD method to carry out the model parameter identification for underwater vehicles. The specific identification method and processes are described as follows.

3.1 Rigid mass and moment

The underwater vehicle in question is a type of remotely operated vehicle (ROV). The mechanical components were modeled and designed using SOLIDWORKS. As shown in Figure 1, the ROV includes three horizontal thrusters and one vertical thruster, and is equipped with perception and navigation sensors such as light-emitting diode (LED) lights, a camera, a P30 ranging sonar, a depth gauge, and an electronic compass. The overall frame is made of 7075 aluminum alloy. In the software, the weight of each component is set based on the weight obtained through weighing or the corresponding material properties. This allows for the assessment of the ROV's weight, center of gravity, and moment of inertia. The center of gravity is marked in Figure 1 as coinciding with the centerline of the horizontal side thrusters. The parameters for weight and moment of inertia are as follows.

$$m = 35.2kg, I_{zz} = 1.38kgm^2 \tag{10}$$

3.2 Computational fluid dynamics control equations

The STAR-CCM+ software is used to calculate the added mass and drag coefficients for the ROV. The control equations for the numerical simulation are as follows.

3.2.1 Continuity equation

The continuity equation is given as (11), where the water flow is considered an incompressible fluid, thus simplifying the continuity equation to (12).

$$\frac{\partial \rho}{\partial t} + \frac{\partial (\rho u)}{\partial x} + \frac{\partial (\rho v)}{\partial y} + \frac{\partial (\rho w)}{\partial z} = 0 \tag{11}$$

$$\frac{\partial u}{\partial x} + \frac{\partial v}{\partial y} + \frac{\partial w}{\partial z} = 0 \tag{12}$$

3.2.2 Navier-Stokes equation

Equation (13) is the time-averaged Navier-Stokes equation (NS equation), where $\overline{u_i}$ and $\overline{u_j}$ represent the components of the time-averaged velocity; u'_i and u'_j are the fluctuations in velocity; $\overline{p}$ denotes the time-averaged pressure; $\overline{f_i}$ is the body force per unit mass.

$$\frac{\partial \overline{u_i}}{\partial t} + \overline{u_j}\frac{\partial \overline{u_i}}{\partial x_j} = \overline{f_i} - \frac{1}{\rho}\frac{\partial \overline{p}}{\partial x_i} + \upsilon \frac{\partial^2 \overline{u_i}}{\partial x_j \partial x_j} - \frac{\partial \overline{u'_i u'_j}}{\partial x_j} \tag{13}$$

3.2.3 DFBI

In this paper, the DFBI approach is used to simulate the motion of a ROV in response to external forces and hydrodynamic forces generated by water flow. STAR-CCM+ calculates the resultant force and torque acting on the rigid body and solves the motion control equations to obtain the velocity state of the ROV.

3.3 Numerical simulation process

This paper employs numerical simulation to calculate the velocity (angular velocity) response of a ROV navigating underwater under the influence of driving forces (torques), aiming to obtain the parameters of the ROV by the optimization algorithm. STAR-CCM+ uses the SIMPLE algorithm to solve the Reynolds-Averaged Navier-Stokes (RANS) equations, and employs dynamic mesh technology and the DFBI approach to solve for the ROV's motion, achieving numerical simulation of the vehicle's four degrees of freedom movement in still water. The overall solution process is presented in Figure 2. The following subsections will illustrate the computational domain, boundary conditions, mesh and physical continuum, and solver settings, taking the example of the ROV moving under the action of a forward force.

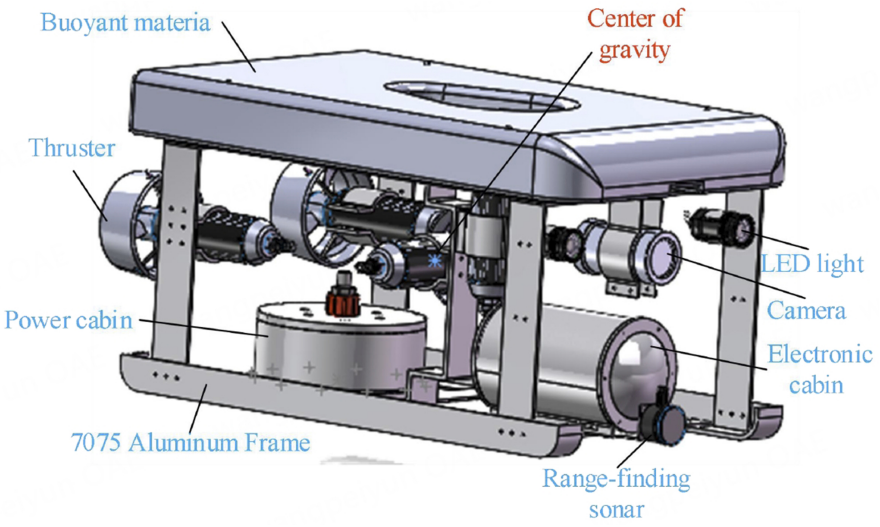

Figure 1. 3D model of ROV created by SOLIDWORKS. ROV: Remotely operated vehicle.

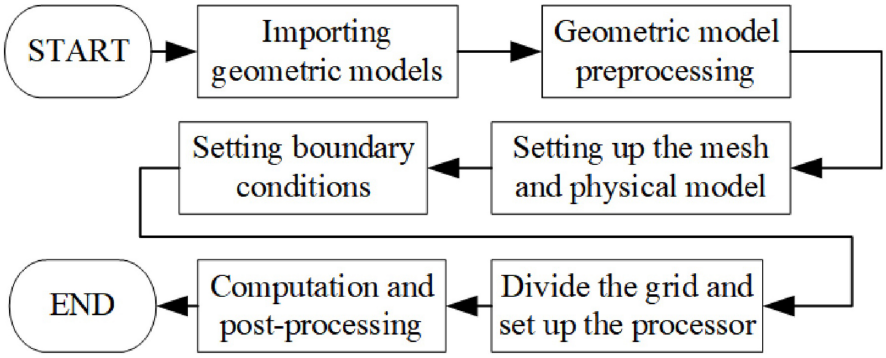

Figure 2. Numerical simulation process.

3.3.1 Calculation of catchment and boundary conditions

The geometric model of the ROV was imported into the STAR-CCM+, and a flow field of 10 m × 5 m × 5 m was set up with the ROV placed in the middle. In the numerical simulation of forward motion, the overset mesh area (3.0 m × 1.4 m × 1.4 m) is set [Figure 3]. The boundaries of the flow field are all set as walls, where the upper boundary is set as a slip wall and the other boundaries are non-slip walls. The overset mesh region is geometrically subtracted from the ROV to obtain the computational domain of the internal motion of the ROV, which is also set as a non-slip wall, and the boundary of the internal computational domain is set as an overset mesh and the overset mesh intersection is established.

3.3.2 Mesh continuum setup and division

The mesh setting has a significant impact on the computational accuracy, and two sets of mesh sizes were set for the main fluid region and the inner domain. The surface remesh, the trimmer mesh, and the prismatic layer were set. The base size of the main region is 0.32 m, with 7 m × 3 m × 3 m grid encryption zones and 0.02 m grid size for the encryption zones. The fluid domain is reasonable. The boundaries of the main flow domain are essentially unaffected by the ROV's motion, with no flow velocity. The basic mesh size for the inner overset domain in motion is set to 0.02 m, with mesh reconstruction enabled on the ROV surface at a size of 0.002 m. The prism layer mesh is 20% of the base size, with six layers and a mesh growth

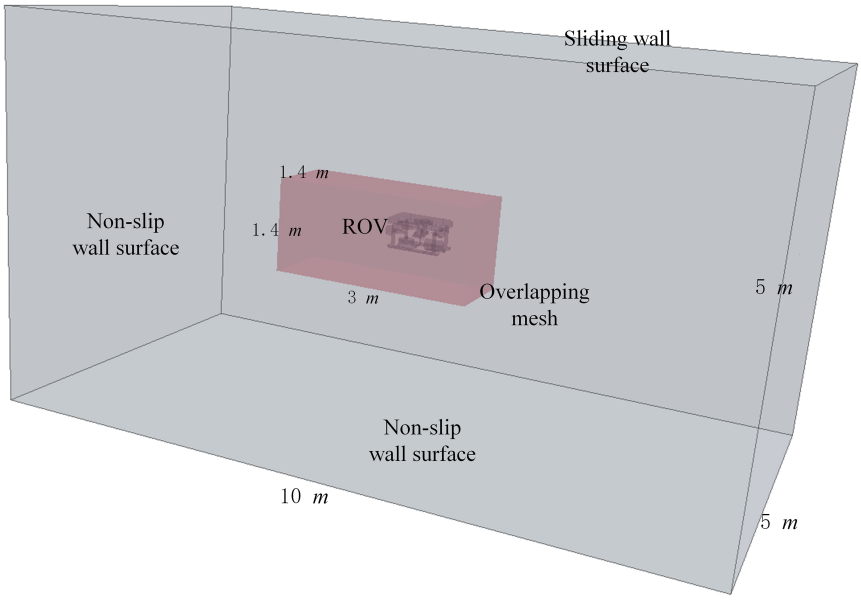

Figure 3. Computational domain under forward force.

rate of 1.2. The template growth rates for both sets of meshes are set to very slow. The mesh division results are shown in Figure 4, with a total of 12,899,038 meshes generated.

3.3.3 Calculation of catchment and boundary conditions

The overset grid and DFBI method are used to obtain the velocity response of the ROV under the action of propulsive force, thereby identifying the inertial and resistance parameters. The physical continuum includes implicit non-stationary, liquid, separated flow, constant density, k - ε turbulence, *etc.*; motion is turned on for DFBI rotation and translation, set to four degrees of freedom motion. The initial parameters, such as center of gravity, mass, rotational inertia, and so on, are also set. At last, the external force (driving force) is turned on to solve the state of motion of the ROV under the action of the external force. The solver time step is set to 0.02 s [$\Delta t = (0.05\sim0.01)\frac{L}{U}$], and the other parameters are kept as default.

3.4 Numerical simulation results

The size and density of the mesh will have an impact on the accuracy of the simulation results and computational efficiency; the grid size and density were determined after considering the movement of the ROV and computational efficiency. The 90 N external force is selected to carry out the grid-independent analysis. We modify the mesh size to generate 5,808,310, 12,899,038, and 26,089,041 grids, respectively. We produced a basin larger than the geometric model, with an increase of 1 m in length, width and height, and the results of the calculations are shown in Figure 5, which are similar to the results of the large basin calculations, verifying the basin-independence. Time-independence was also investigated but was not shown in the figure because the resulting curves were too similar. The results of the grid set in this work are basically the same as the finer grid (26,089,041 grid), with a maximum speed deviation of less than 0.19 calculation accuracy requirements. Therefore, in order to speed up the calculation, the numerical simulation calculation for each working condition was carried out by dividing the grid with the parameters described in Section 3.3.2.

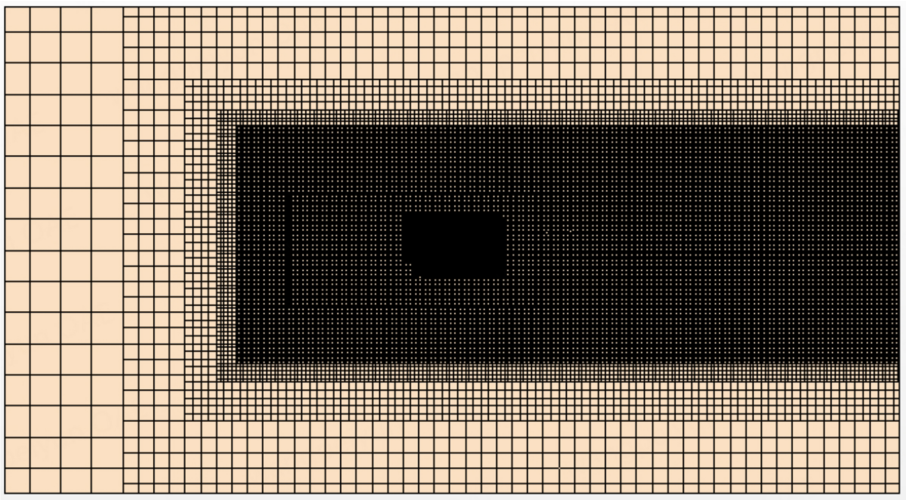

Figure 4. Grid partitioning.

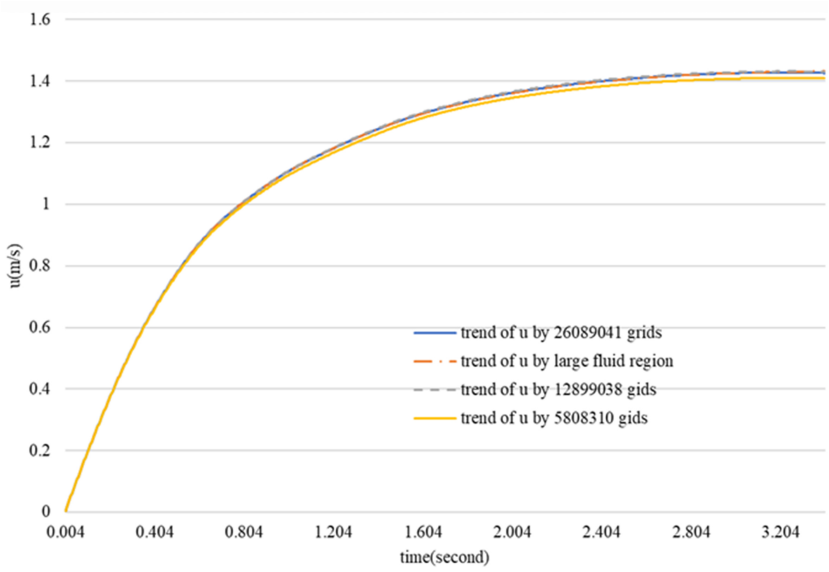

Figure 5. Velocity responses of ROV under different grid quantities. ROV: Remotely operated vehicle.

The plots obtained from the calculation of 90 N forward force are shown in Figures 6 and 7, including the velocity and pressure plots. In the simulation of forward motion, the forward force is set as 2 N, 5 N, and one force is selected at 10 N intervals from 10 to 100 N, for a total of 13 calculation cases. The velocity and acceleration responses of the ROV under each force condition are obtained through numerical simulation, totaling 15,320 data, which reflect the relationship between velocity, acceleration and force.

Numerical simulations of velocity and acceleration were also carried out under the effect of transverse and vertical forces and turning moments. A total of 52,690 data were obtained from the numerical simulation of the applied forces on each degree of freedom, and the following parameter identification was carried out based on the data obtained from the simulation calculations.

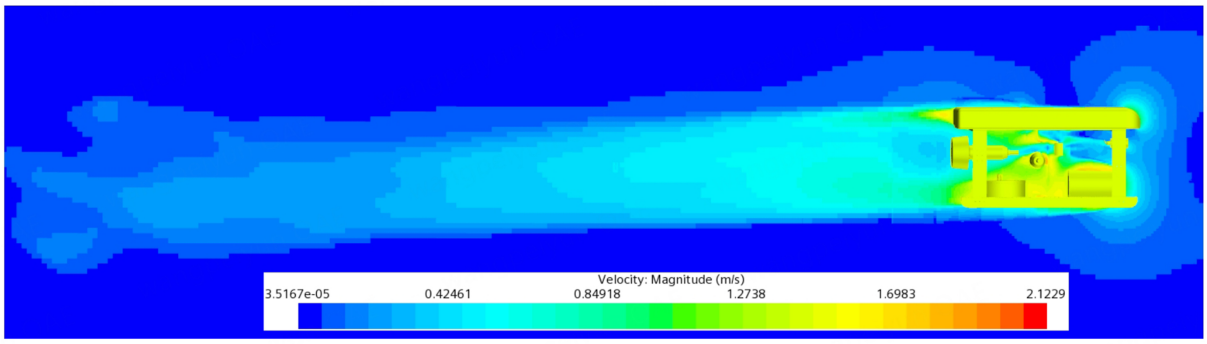

Figure 6. Velocity map of numerical simulation under 90 N forward force.

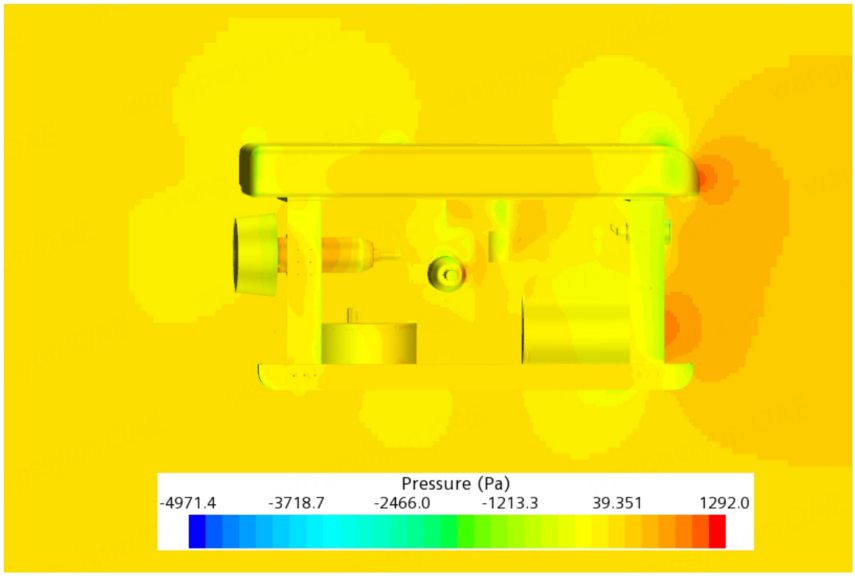

Figure 7. Pressure map of numerical simulation under 90 N forward force.

3.5 Parameter identification by QPSO

After determining M_{RB} through SOLIDWORKS, the main purpose of parameter identification is to determine the inertia parameter and the primary and secondary drag parameters in M_A, $D(v)$ and to establish the dynamics model of the robot. In this paper, under the condition of four degrees of freedom without decoupling, the inertial parameters $X_{\dot{u}}$, $Y_{\dot{v}}$, $Z_{\dot{w}}$, $N_{\dot{r}}$, primary resistance parameters X_u, Y_v, Z_w, N_r, and secondary resistance parameter $X_{u|u|}$, $Y_{v|v|}$, $Z_{w|w|}$, $N_{r|r|}$ are identified and optimized simultaneously using the data from numerical simulations. The fitness function for optimization is as per Equation (14), where K = 52,690. (14) can be obtained by substituting the velocity and acceleration values into Equation (2) to obtain the driving force τ_{id} under that set of parameters, and comparing it with the real driving force τ of the corresponding velocity and acceleration.

$$f(p) = \sum_{i=1}^{K} |\tau_i - \tau_{id}| / \sqrt{K} \tag{14}$$

The QPSO algorithm has few control parameters, strong global search capability, simple equations of particle motion, and relatively few computations per iteration. Therefore, this algorithm is selected for parameter identification in this paper. The QPSO algorithm parameter identification process is as follows:

(1) Initialization: set the population size M, the dimension N, and randomly generate the initial position of each particle p_i;
(2) Calculate the average optimal position of all particles $mbest = \sum_{i=1}^{M} p_i/M$ and fitness value of each particle;
(3) Update the local optimal fitness value of individual particles, and update the global optimal fitness value: $g = \arg\min_{1\le i\le M}(f(p_i))$ and get the best particle p_g;
(4) Calculate learning tendency points: $p_d = \varphi^* p_i + (1 - \varphi)^* p_g, \varphi \in U(0, 1)$, and update particle position: $p_i = p_d \pm \beta * |mbest - p_i| * \ln(1/u), u \in U(0, 1)$;
(5) Check the termination condition (usually the maximum number of iterations is reached or the fitness value has not been updated for many iterations); if it is satisfied, then end; otherwise, go to (2) for the next iteration. This section shows the main findings of our study. It may contain conclusive description, analysis, and comparison with other related research results, *etc.*

4. EXPERIMENTAL VERIFICATION

Parameter identification was carried out using the QPSO algorithm based on the data from the numerical simulation, and the identification results are shown in Table 1. PSO, GA, and the least squares method were also used to identify the parameters of the numerical simulation data, and the identification results on the forward direction of the robot are shown in Table 2.

Experiments in the pool were carried out to obtain the velocity response of the robot under maximum forward thrust in order to verify the accuracy of the identification method proposed in this paper. After the parameter identification, a dynamics model is established, and the velocity response under the maximum forward thrust is solved and compared with the experimental data.

4.1 Experimental setup

The experimental site is an open-air pool [Figure 8]. In this paper, an UWB positioning system is used to measure the position of the underwater vehicle, from which the speed is inferred.

As shown in Figure 8, the four base station beacons (A, B, C, and D) of the UWB localization system were placed at the four corners of the pool during the experiment, so that the whole pool was included in the measurement range of the localization system, and the localization module (E) of the UWB was equipped on the underwater vehicle by means of the risers, as shown on the left in Figure 9. Before using the UWB positioning system, the distances from base stations B, C, and D to the main base station A were recorded into the software, which facilitated the real-time output of the underwater vehicle's position based on the distances of the four base stations. The underwater vehicle is also equipped with a nine-axis high-precision sensor to provide attitude angle and three-axis acceleration, which can be used to calibrate the experimentally acquired velocities.

Because the designed robot is not equipped with a Doppler velocimeter and there may be some errors when using the UWB localization module system alone. To further improve the accuracy of the experimentally obtained speed, this paper employs an M900 dual-frequency multibeam imaging sonar (as shown in the right image of Figure 9) to record the motion state of the underwater vehicle. The M900 sonar is fixed underwater, and its working frequency is set to 900 kHz, with a scanning opening angle set to 130°, to start observing the movement of the ROV. The M900 outputs an image every 200 ms, and by calculating the distance the ROV moves between two frames, the speed of the ROV within 200 ms can be determined. Thus, sonar can be used as a second source of velocity observations. This speed is then used to validate and integrate with the speed data measured by the positioning system.

Table 1. Result of parameter identification

Parameter (unit)	Value
Additional mass (kg); additional inertia (kg*m^2)	$X_{\dot{u}}$ = -16.04, $Y_{\dot{v}}$ = -37.74, $Z_{\dot{w}}$ = -83.60, $N_{\dot{r}}$ = -1.06
Linear resistance (Ns/m; Ns/rad)	X_u = -2.41, Y_v = -1.50, Z_w = -21.75, N_r = -1.18
Secondary resistance (Ns^2/m^2; Ns^2/rad^2)	$X_{\|u\|u}$ = -44.17, $Y_{\|v\|v}$ = -114.30, $Z_{\|w\|w}$ = -121.30, $N_{\|r\|r}$ = -2.64

Table 2. Other algorithm recognition results

Parameter (unit)	PSO	GA	Least squares method
Additional mass (kg); additional inertia (kg*m^2)	$X_{\dot{u}}$ = -9.90	$X_{\dot{u}}$ = -16.15	$X_{\dot{u}}$ = -16.07
Linear resistance (Ns/m; Ns/rad)	X_u = -3.55	X_u = -1.98	X_u = -2.21
Secondary resistance (Ns^2/m^2; Ns^2/rad^2)	$X_{\|u\|u}$ = -45.30	$X_{\|u\|u}$ = -44.56	$X_{\|u\|u}$ = -44.42

PSO: Particle swarm optimization; GA: genetic algorithm.

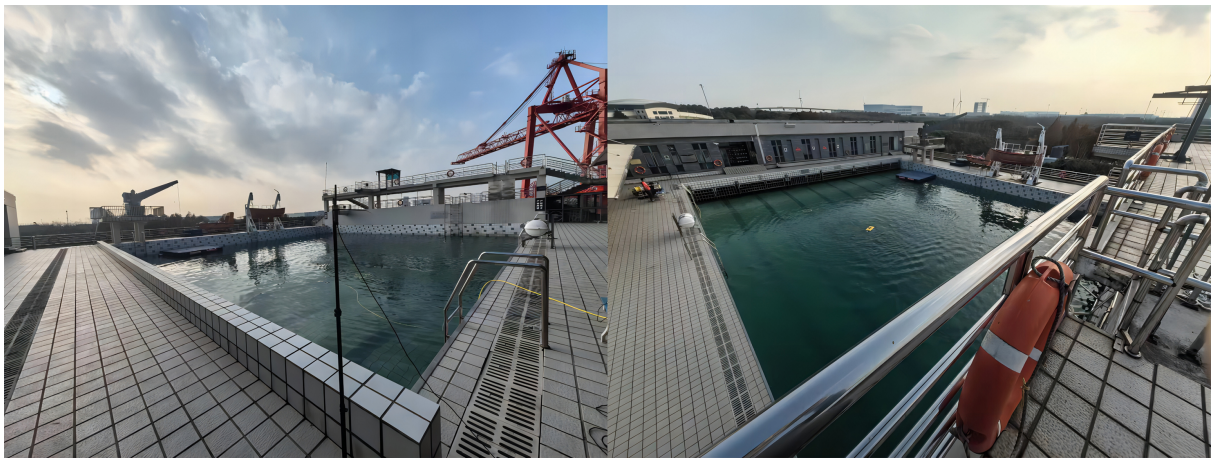

Figure 8. Experimental environment settings.

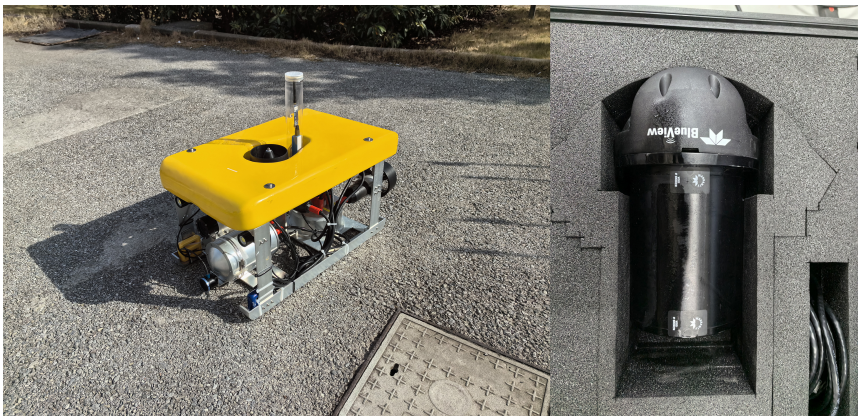

Figure 9. ROV with positioning module and sonar. ROV: Remotely operated vehicle.

4.2 Experimental results and comparison

The forward speed response observed in the experiment is shown as the green curve in Figure 10. With the horizontal thrusters operating at maximum force output in the forward direction, the ROV's maximum

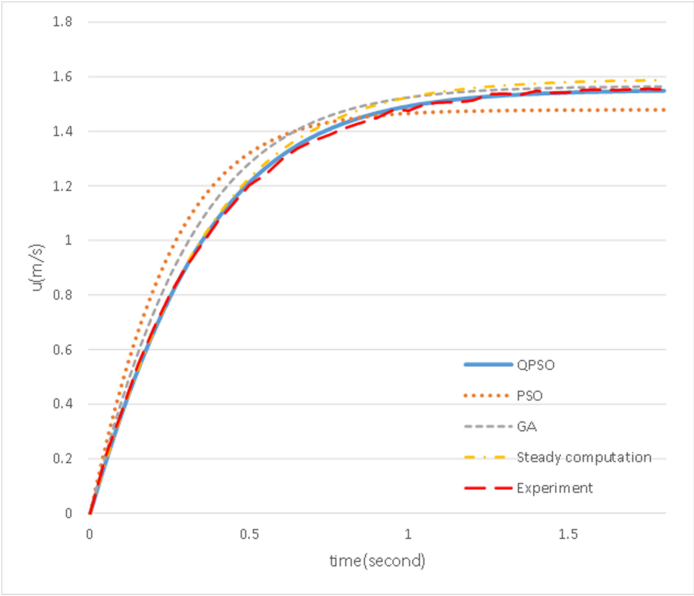

Figure 10. Velocity response of ROV. ROV: Remotely operated vehicle.

speed is approximately 1.55 m/s. The red dotted line in the figure represents the speed response predicted by the ROV model established based on parameters identified using QPSO, which best fits the experimental data. The root mean square error of the speed is 0.2%.

Parameter identification based on PSO, GA, Q-learning[22] and the least squares method with decoupled ROV's motion freedom is also carried out in this paper. The curves recognized by the Q-learning algorithm are not shown in the figure as they are not highly distinguishable from algorithms other than QPSO. PSO and GA are often considered as traditional optimization algorithms. They are still widely used in many fields and have their own unique advantages and application scenarios. The error of the ROV's numerical simulation model built based on the least-squares method with decoupled ROV's motion freedom is 0.55%, which is larger than that of the DFBI combined with the QPSO identification method proposed in this paper. Although PSO and GA also use the data from DFBI numerical simulation to search for the optimal identification of ROV models, the optimization effect is poorer than that of QPSO, and the errors of the established models are PSO: 1.42% and GA: 0.84%, which are prone to fall into premature or locally optimal solutions in the optimization search.

5. CONCLUSION

The establishment of an accurate underwater vehicle model from underwater vehicle parameter identification is of great significance for its controller design. In this paper, based on the DFBI numerical simulation method in CFD and combined with the QPSO algorithm, we propose a method to identify the inertia and drag parameters of the four degrees of freedom of the underwater vehicle at the same time. After the experimental comparison (the root mean square error is less than 0.20%). Through the comparison of different algorithms, the accuracy of the proposed method is verified, which can provide a reference for researchers to identify the hydrodynamic parameters of the ROV.

DECLARATIONS

Authors' contributions

Developed the ROV, carried out the numerical simulation, and wrote the QPSO program: Chen M
Wrote the PSO code and the draft: Liu Y
Organized the experiment, guided the work, and wrote the least-squares codes: Zhu D
Wrote the GA codes: Wang C
Helped collect and process the data: Ji K

Availability of data and materials

Not applicable.

Financial support and sponsorship

This work was supported in part by the National Natural Science Foundation of China (52371331, 62033009).

Conflicts of interest

Zhu D and Chen M are the guest editors of the Special Issue of "Updates in Underwater Robotics", and Zhu D is an Editorial Board Member of the journal *Intelligence & Robotics*, while the other authors have declared that they have no conflicts of interest.

Ethical approval and consent to participate

Not applicable.

Consent for publication

Not applicable.

REFERENCES

1. Banerjee I, Pangule RC, Kane RS. Antifouling coatings: recent developments in the design of surfaces that prevent fouling by proteins, bacteria, and marine organisms. *Adv Mater* 2011;23:690-718. DOI
2. Chen M, Zhu D, Pang W, Chen Q. An effective strategy for distributed unmanned underwater vehicles to encircle and capture intelligent targets. *IEEE T Ind Electron* 2024:1-11. DOI
3. Xu F, Zou ZJ, Yin JC, Cao J. Identification modeling of underwater vehicles' nonlinear dynamics based on support vector machines. *Ocean Eng* 2013;67:68-76. DOI
4. Luque JCC, Donha DC, de Barros EA. AUV parameter identification. *IFAC Proc Vol* 2009;42:72-7. DOI
5. Huajun Z, Xinchi T, Hang G, Shou X. The parameter identification of the autonomous underwater vehicle based on multi-innovation least squares identification algorithm. *Int J Adv Robot Syst* 2020;17:1729881420921016. DOI
6. Ahmed F, Xiang X, Jiang C, Xiang G, Yang S. Survey on traditional and AI based estimation techniques for hydrodynamic coefficients of autonomous underwater vehicle. *Ocean Eng* 2023;268:113300. DOI
7. Wang D, Wan J, Shen Y, Qin P, He B. Hyperparameter optimization for the LSTM method of AUV model identification based on Q-learning. *J Mar Sci Eng* 2022;10:1002. DOI
8. de Ven PWJ, Johansen TA, Sørensen AJ, Flanagan C, Toal D. Neural network augmented identification of underwater vehicle models. *IFAC Proc Vol* 2004;37:263-8. DOI
9. Chocron O, Vega EP, Benbouzid M. Dynamic reconfiguration of autonomous underwater vehicles propulsion system using genetic optimization. *Ocean Eng* 2018;156:564-79. DOI
10. Cardenas P, de Barros EA. Estimation of AUV hydrodynamic coefficients using analytical and system identification approaches. *IEEE J Oceanic Eng* 2020;45:1157-76. DOI
11. Lin M, Yang C, Li D. Hybrid strategy based model parameter estimation of irregular-shaped underwater vehicles for predicting velocity. *Robot Auton Syst* 2020;127:103480. DOI
12. Prawin J, Rao ARM, Lakshmi K. Nonlinear parametric identification strategy combining reverse path and hybrid dynamic quantum

particle swarm optimization. *Nonlinear Dynam* 2016;84:797-815. DOI

13. Sun B, Pang W, Chen M, Zhu D. Development and experimental verification of search and rescue ROV. *Intell Robot* 2022;2:355-70. DOI
14. Zhou G, Xiang X, Liu C. Parameter identification and model prediction path following control of underactuated AUV: methodology and experimental verification. *Control Eng Pract* 2023;141:105729. DOI
15. Hong L, Fang R, Cai X, Wang X. Numerical investigation on hydrodynamic performance of a portable AUV. *J Mar Sci Eng* 2021;9:812. DOI
16. Bentes C. Modeling of an autonomous underwater vehicle. 2016. Available from: https://api.semanticscholar.org/CorpusID:198363077 . [Last accessed on 25 Jun 2024].
17. Wang C, Zhang F, Schaefer D. Dynamic modeling of an autonomous underwater vehicle. *J Mar Sci Technol* 2015;20:199-212. DOI
18. Bao H, Zhu H. Modeling and trajectory tracking model predictive control novel method of AUV based on CFD data. *Sensors* 2022;22:4234. DOI
19. Li J, Wang Y, Di F. Model identification method of intervention AUV system based on numerical simulation. In: Second International Conference on Mechanical Design and Simulation (MDS 2022); Wuhan, China. pp. 953-69. DOI
20. Fossen TI. Handbook of marine craft hydrodynamics and motion control. 2011. DOI
21. Luo YH, Wu JM, Zhou HF. Trajectory tracking control of underwater vehicle based on hydrodynamic parameters calculated by CFD. *Chin J Ship Res* 2022;17:237-45,272. DOI
22. Shi W, Song S, Wu C, Chen CLP. Multi pseudo Q-learning-based deterministic policy gradient for tracking control of autonomous underwater vehicles. *IEEE Trans Neural Netw Learn Syst* 2019;30:3534-46. DOI